Current Biology 20, 914–920, May 25, 2010 ©2010 Elsevier Ltd All rights reserved DOI 10.1016/j.cub.2010.03.057

Report

An *S*-Acylation Switch of Conserved G Domain Cysteines Is Required for Polarity Signaling by ROP GTPases

Nadav Sorek,[1] Oshik Segev,[2] Orit Gutman,[3] Einat Bar,[4] Sandra Richter,[5] Limor Poraty,[1] Joel A. Hirsch,[2] Yoav I. Henis,[3] Efraim Lewinsohn,[4] Gerd Jürgens,[5] and Shaul Yalovsky[1,*]

[1]Department of Molecular Biology and Ecology of Plants
[2]Department of Biochemistry
[3]Department of Neurobiology
George S. Wise Faculty of Life Sciences, Tel Aviv University, Tel Aviv 69978, Israel
[4]Department of Field and Vegetable Crops, Agricultural Research Organization, Neve Ya'ar Reseach Center, P.O. Box 1021, Ramat Yishay 30095, Israel
[5]Center for Plant Molecular Biology, University of Tübingen, D-72076 Tübingen, Germany

Summary

Rho GTPases are master regulators of cell polarity [1]. For their function, Rhos must associate with discrete plasma membrane domains [2]. Rho of Plants (ROPs) or RACs comprise a single family [3–5]. Prenylation and *S*-acylation of hypervariable domain cysteines of Ras and Rho GTPases are required for their function [6–11]; however, lipid modifications in the G domain have never been reported. Reversible *S*-acylation involves the attachment of palmitate (C16:0) or other saturated lipids to cysteines through a thioester linkage and was implicated in the regulation of signaling [12]. Here we show that transient *S*-acylation of *Arabidopsis* AtROP6 takes place on two conserved G domain cysteine residues, C21 and C156. C21 is relatively exposed and is accessible for modification, but C156 is not, implying that its *S*-acylation involves a conformational change. Fluorescence recovery after photobleaching beam-size analysis [13] shows that *S*-acylation of AtROP6 regulates its membrane-association dynamics, and detergent-solubilization studies indicate that it regulates AtROP6 association with lipid rafts. Site-specific acylation-deficient AtROP6 mutants can bind and hydrolyze GTP but display compromised effects on polar cell growth, endocytic uptake of the tracer dye FM4-64, and distribution of reactive oxygen species. These data reveal an *S*-acylation switch that regulates Rho signaling.

Results and Discussion

Previously, we showed that an *Arabidopsis* ROP, AtROP6 (designated throughout as ROP6), undergoes activation-dependent transient *S*-acylation by palmitic (C16:0) or stearic (C18:0) acids and consequent partitioning into detergent-resistant membranes (DRMs) that could reflect association with lipid rafts [11].

The sequence of ROP6 was analyzed to identify potential *S*-acylated cysteines. Aside from the geranylgeranylated CaaL box C196 [11], there are three cysteine residues in the ROP6 G domain, at positions 9, 21, and 156. Previously, we showed that the association of a constitutively active (CA) rop6^{CA} C156S (rop6^{CA156mS}) mutant with DRM was reduced, suggesting that it may be *S*-acylated [4, 9–11]. In addition, C21, which is located on helix α1, is relatively exposed to the medium and could also be an acyl group acceptor (Figure 1A). The G domain of ROPs is highly similar to that of nonplant Rho GTPases [14]. Indeed, both C21 and C156 are highly conserved among all plant ROP and Rho family proteins in diverse organisms (see Figure S1 available online). Examination of ROP9 structure (PDB 2J0V) reveals that C21 and C156 are at the nucleotide-binding site (Figure 1B). C21 faces the solvent with its thiol accessible for *S*-acylation. However, C156 is buried at the bottom of the nucleotide-binding pocket and thus requires a conformational change to expose its thiol group for *S*-acylation.

Nucleotide binding (Figure 1C) and GTPase assays (Figure 1D) were performed to exclude the possibility that mutations in C21, C156, or both affect GTP binding and hydrolysis. A recombinant CA ROP6 mutant (rop6^{CA}) [11] and a CA mutant in which C21 and C156 were changed into serines (rop6$^{CA21+156mSS}$) were purified from *E. coli*. The bound nucleotide was released and identified by reverse-phase high-performance liquid chromatography (HPLC) [15] (Figure 1C; see Supplemental Experimental Procedures). GDP or GTP in the same buffer served as standards. Both rop6^{CA} and rop6$^{CA21+156mSS}$ were bound to GTP with only a residual amount of GDP (Figure 1C), indicating that mutating C21 and C156 to serines did not affect nucleotide binding. The slight difference that can be seen in the HPLC absorbance units is within the error range of the machine and does not reflect a difference in nucleotide levels.

Wild-type (WT) ROP6 and a C21S;C156S double mutant (rop6$^{21+156mSS}$) hydrolyzed GTP at similar rates (Figure 1D), with hydrolysis constants (K_{hyd}) (L/[mol × min]) [16] of 342 and 316, respectively. In contrast, both rop6^{CA} and rop6$^{CA21+156mSS}$ CA mutants purified from either *E. coli* or *Arabidopsis* did not hydrolyze GTP (Figure 1D). Thus, mutating C21 and C156 to serines did not affect GTP binding and hydrolysis.

Previously, we established a link between ROP activation, *S*-acylation, and partitioning into lipid rafts [11]. Because the C21S;C156S double mutation did not affect GTP binding and hydrolysis, we reasoned that mutants in either or both cysteines could be used to identify the acyl acceptor and the importance of *S*-acylation for ROP function. Transgenic *Arabidopsis* lines constitutively expressing the following His- and GFP-tagged ROP6 mutants were created: His_6-GFP-rop^{CA} (rop6^{CA}), His_6-GFP-rop6^{CA} C21S mutant (rop6^{CA21mS}), His_6-GFP-rop6^{CA} C156S mutant (rop6^{CA156mS}), and His_6-GFP-rop6^{CA} C21S; C156S double mutant (rop6$^{CA21+156mSS}$). For each of WT and four mutants, three independent transgenic lines, which showed similar protein expression levels, were selected for further analysis (Figure S2E). The analysis was carried out in parallel on all 15 lines.

S-acylation was determined by gas chromatography-coupled mass spectrometry (GC-MS) [11, 17]. The relative *S*-acylation levels were compared to rop6^{CA} (Figure 2A; Figures S4F–S4H). The GC-MS analysis showed that both

*Correspondence: shauly@tauex.tau.ac.il

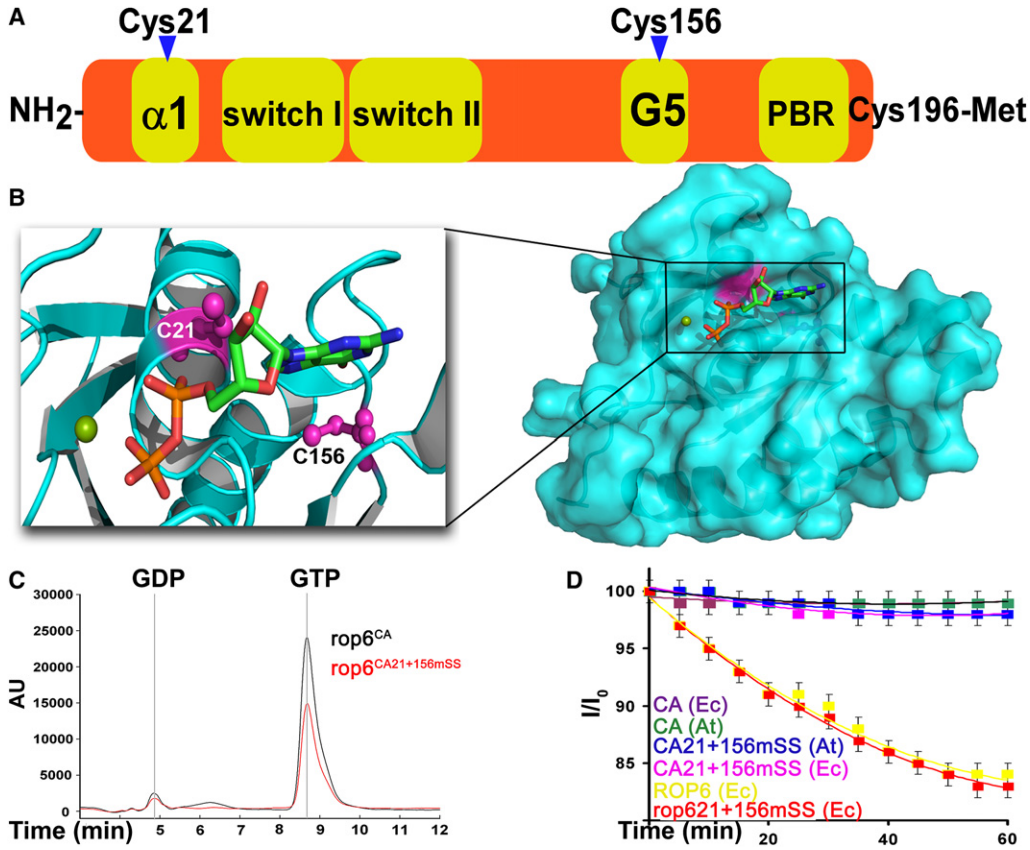

Figure 1. G Domain Cysteines 21 and 156 Are Not Required for GTP Binding and Hydrolysis

(A) A scheme of *Arabidopsis* ROP6 highlighting C21, C156, and the prenylated CaaL box C196.

(B) Structure of AtROP9 (PDB 2J0V) bound to Mg^{2+} (green sphere)-GDP (sticks), highlighting C21 and C156 (ball and sticks) in pink and the nucleotide-binding pocket. The surface representation is color-coded as in the cartoon representation; C156 is not easily seen as a result of the perspective and burial. Models were drawn with PyMOL (http://pymol.org/).

(C) Identity of nucleotides released from constitutively active $rop6^{CA}$ and $rop6^{CA21+156mSS}$ determined by reverse-phase high-performance liquid chromatography (HPLC).

(D) GTPase assays showing that ROP6 and the double cysteine mutant $rop6^{21+156mSS}$ hydrolyzed GTP at approximately the same rate with K_{hyd} of 342 and 316, respectively. No GTP hydrolysis was observed in constitutively active (CA) $rop6^{CA}$ and $rop6^{CA21+156mSS}$ (CA21+156mSS) that were purified from either *E. coli* (Ec) or *Arabidopsis* (At). The following abbreviations are used: AU, HPLC absorbance units; I_0, the initial GTP amount (50 nmol); I, I_0 − measured released Pi. The y axis scale is $I/I_0 \times 100$. For more information, see Figure S1.

C21 and C156 are *S*-acylated. The mutation in C21 reduced the *S*-acylation level by 30%, the mutation in C156 reduced it by 66%, and no *S*-acylation was detected in the C21S;C156S double mutant $rop6^{CA21+156mSS}$ (Figure 2B). The differences in *S*-acylation and the additive effect of the mutations in C21 and C156 suggest that a subpopulation of ROP6 is *S*-acylated only on C156, whereas both C21 and C156 are modified in a smaller subpopulation. Alternatively, there may be two populations modified in either cysteine; the majority of ROP6 molecules would then be *S*-acylated on C156 and in a smaller population on C21. Currently, we are unable to differentiate between the two options.

Next, we examined the effect of *S*-acylation on ROP membrane localization and dynamics. Subcellular localization of endogenous ROPs was tested by immunostaining of root cell division zone with polyclonal α-ROP6 antibodies, which recognize both type I and type II ROPs [11]. The ROPs were localized at the plasma membrane together with the plasma membrane marker GFP-LTi and separate from the *Golgi* marker GFP-Nag [18] (Figure 3A). Rho GTPase activation status assays were carried out to test whether activated endogenous ROPs partition into lipid rafts. These assays employed ICR1 (interactor of constitutively active ROPs 1), which preferentially interacts with GTP-bound ROPs [19]. GST-ICR1-conjugated resin was used to pull down endogenous ROPs from either detergent-soluble membranes (SM) or DRM. Higher amounts of ROPs were pulled down by GST-ICR1 from DRM compared to SM fractions, although the levels of ROPs in either fraction were similar (Figure 3B). Previously, we showed that ROPs equally partition between DRM and SM and that ROP6 was prenylated and *S*-acylated in DRM but only prenylated in SM [11]. Together with these previous data, the immunostaining (showing plasma membrane localization) and activation status assays in SM and DRM fractions provide a link between ROP activation, transient *S*-acylation, and partitioning into lipid rafts.

To further test the role of transient *S*-acylation in ROP membrane localization, we determined the subcellular localization of the different His_6-GFP-ROP6 mutants (Figures 3C and 3D). Analysis of protein distribution with a confocal laser scanning microscope (CLSM) showed that His_6-GFP-ROP6, His_6-GFP-$rop6^{CA}$, His_6-GFP-$rop6^{CA21mS}$, His_6-GFP-$rop6^{CA156mS}$, and His_6-GFP-$rop6^{CA21+156mSS}$ are localized at

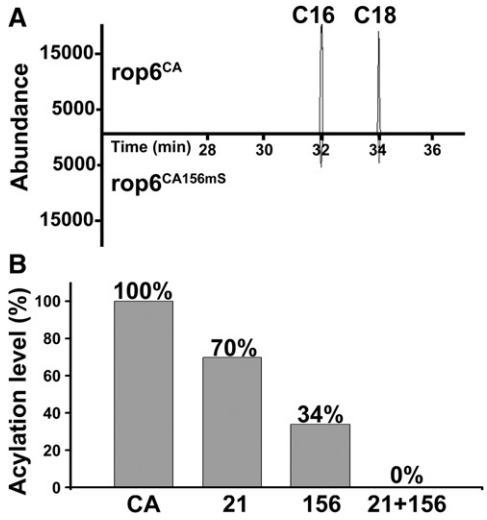

Figure 2. ROP6 Is *S*-Acylated by Palmitic and Stearic Acid on Both Cysteine 21 and Cysteine 156

(A) Gas chromatography chromatograms showing palmitoylation and stearylation levels of His_6-GFP-rop6^{CA} and His_6-GFP-rop6^{CA156mS} purified from transgenic *Arabidopsis* plants. C16 and C18 correspond to palmitic and stearic acids, respectively.

(B) Quantification of the *S*-acylation levels. For more information, see Figure S2 and Figure S4.

the plasma membrane (Figure 3C). Membrane flotation-centrifugation was used to further substantiate the CLSM data and determine the distribution of ROP6 mutants between DRM and SM fractions (Figure 3D); this distribution correlated with the *S*-acylation status of the mutants (Figure 2). ROP6 partitioned equally between SM and DRM. rop6^{CA} was exclusively localized in DRM, versus only 76% of rop6^{CA21mS}. In contrast, only 28% of rop6^{CA156mS} was localized in DRM. The C21S;C156S double mutant rop6$^{CA21+156mSS}$ partitioning between DRM and SM fractions was 2% versus 98%, respectively. Together with previously published data [9–11], the results in Figure 2 and Figures 3C and 3D revealed that the transient *S*-acylation of G domain C21 and C156 is required for association with lipid rafts, but not for targeting to the plasma membrane.

To ensure that subcellular localization and *S*-acylation of ROP6 and rop6^{CA} were not affected by their overexpression, we examined the localization and *S*-acylation of ROP6 and rop6^{CA} expressed under the *ROP6* promoter (*pROP6* > > GFP-ROP6; *pROP6* > > GFP-rop6^{CA}) (Figures S2A and S2B). Similar to overexpressed ROP6 and rop6^{CA}, ROP6 and rop6^{CA} expressed from the *pROP6* promoter were detected in the plasma membrane (Figures S2A and S2B) and were *S*-acylated by palmitic and stearic acids (Figures S2C and S2D).

The activation status-dependent partitioning of ROPs within and outside of lipid rafts suggested that transient *S*-acylation might regulate the dynamics of ROPs in the membrane. We therefore used florescence recovery after photobleaching (FRAP) beam-size analysis [13] to measure the dynamics of ROP6 interactions with the plasma membrane of living cells. The method employs FRAP with two different laser beam sizes, both small enough such that diffusion in the cytoplasm is instantaneous and does not contribute to the measurement, to measure the relative contribution of lateral diffusion and membrane-cytoplasm exchange to the fluorescence recovery. The method and statistical analyses are described in the Supplemental Experimental Procedures, along with typical FRAP experiments (Figure S3). The ratio between the areas illuminated by the Gaussian laser beam focused through a 63× or a 40× objective, $\omega^2(40\times)/\omega^2(63\times)$ (where ω is the Gaussian radius), was 2.28. For FRAP by lateral diffusion, the ratio between the characteristic recovery time (τ) values measured with the two beam sizes, $\tau(40\times)/\tau(63\times)$, equals the ratio between the illuminated areas; on the other hand, a τ ratio of 1 is indicative of recovery by exchange, which is a chemical relaxation process whose rate is independent of the beam size [13]. The τ ratio is determined by the relative rates of diffusion and exchange; thus, either enhanced exchange or slower diffusion would shift the τ ratio from 2.28 toward 1, with the faster of the two processes having a higher contribution [13]. The beam-size analysis (Figures 3E and 3F) showed that ROP6 membrane interactions depend on its *S*-acylation. WT ROP6 exhibited a $\tau(40\times)/\tau(63\times)$ ratio of 2.0, close to but smaller than the 2.28 ratio typical of lateral diffusion, suggesting a major contribution of lateral diffusion and a minor contribution of exchange [20]. The CA rop6^{CA} mutant recovered by pure diffusion (τ ratio of 2.29), suggesting a reduction in its exchange rate. On the other hand, the rop6$^{CA21+156mSS}$ double mutant had a τ ratio of 1.4 (Figures 3E and 3F), suggesting a significant increase in its exchange rate relative to lateral diffusion, in line with the notion that the missing *S*-acylation sites contribute to the membrane association of ROP6 in general, and not only to its partitioning into raft domains shown in Figure 3D. A potential contribution of altered interactions of the *S*-acylation mutant with guanine nucleotide dissociation inhibitors (GDIs) cannot be excluded. However, studies on H- and N-Ras, whose membrane association does not depend on GDI, have shown that palmitoylation is required to stabilize their interactions with the plasma membrane [6, 8, 20, 21], supporting the notion that *S*-acylation plays a role in stabilizing ROP6 membrane interactions. It should be noted that the FRAP beam-size analysis gives a direct measure of the relative kinetics of exchange and lateral diffusion and is therefore able to detect the increase in the exchange rate of rop$^{CA21+156mSS}$ under conditions in which the differences are too subtle to be detected by steady-state immunological or confocal techniques.

To gain insight into the role of *S*-acylation in the regulation of cell polarity and growth, we examined the well-documented effects of ROPs on the structure of root hairs (RHs) and leaf epidermis pavement cells [4, 22, 23] and measured the rate of tracer dye (FM4-64) endocytosis [22] and the distribution of reactive oxygen species (ROS) in RH [24] (Figure 4). Similar to other ROPs [22, 23], overexpression of rop6^{CA} induced development of swollen RHs (Figures 4A and 4B) with inhibition of FM4-64 endocytic uptake (Figures 4A and 4C). CM-H_2DCFDA (5 [and 6]-chloromethyl-2′,7′-dichlorodihydro fluorescein) (DCF)-labeled ROS was distributed throughout the cells instead of forming a tip-focused gradient (Figures 4A and 4D).

Quantitative analyses were carried out to determine the effect of ROP6 mutants on cell polarity. The average length of RHs in WT nontransgenic plants was 750 μm, versus 90 μm in swollen *rop6^{CA}* (Figure 4B). The average length of RHs in transgenic plants expressing WT ROP6 was 650 μm. The average length of C21S and C156S single and double mutant RHs was 310 μm in *rop6^{CA21mS}*, 450 μm in *rop6^{CA156mS}*, and 570 μm in *rop6$^{CA21+156mSS}$* (Figure 4B). The differences between the different lines were significant; $p \leq 0.01$ (analysis of variance [ANOVA]).

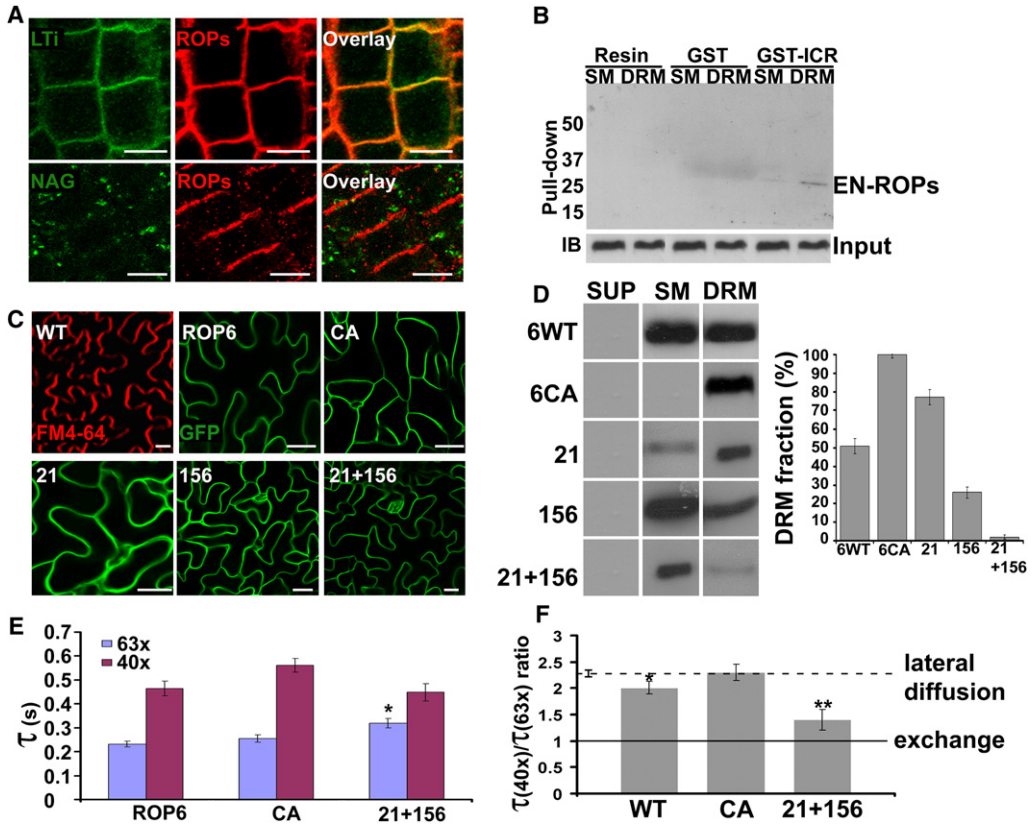

Figure 3. *S*-Acylation of C21 and C156 Is Required for ROP6 Association with Lipid Rafts and for Stable Association with the Plasma Membrane

(A) Immunostaining showing colocalization of ROPs (red) with the plasma membrane marker LTi-GFP, but not with the *Golgi* marker GFP-Nag (green), in the root cell division zone.

(B) Rho GTPase activation assays with GST-ICR1 to pull down GTP-bound ROPs from either detergent-soluble membranes (SM) or detergent-resistant membranes (DRMs). Note the more strongly activated ROP signal associated with DRM. The following abbreviations are used: En-ROPs, endogenous ROPs; input, ROP levels in each fraction. Bottom: control immunoblots showing ROP levels in SM and lipid raft fractions. The two bands in the GST lanes are due to unspecific labeling of the GST protein by the antibodies.

(C) Confocal images showing subcellular localization of His_6-GFP-ROP6 (ROP6-WT, CA, C21S, and C156S single and double mutants). WT-FM4-64 labeled nontransgenic wild-type (WT) plants. Bars correspond to 15 μm in (A) and 20 μm in (C).

(D) Protein immunoblots showing distribution of His_6-GFP-ROP6 WT and mutants between soluble and membrane fractions, DRM, and SM. Error bars represent standard error (SE). For more information, see also Figure S2.

(E) Recovery time (τ) values obtained with fluorescence recovery after photobleaching (FRAP) beam-size analysis with 40× (gray; ω = 1.17 μm) and 63× (blue; ω = 0.77 μm) objectives. The $\omega^2(40\times)/\omega^2(63\times)$ ratio was 2.28. The fluorescence recovery values were high in all cases ($\geq$0.93). Typical FRAP curves are shown in Figure S3. Bars are means ± standard error of the mean (SEM) of 35 measurements. Comparing τ values measured with the same objective, asterisks indicate a significant difference from the value obtained for ROP6 (**$p \leq 10^{-3}$; Student's t test).

(F) Ratios of the τ values shown in (E). Top and bottom lines correspond to FRAP by pure lateral diffusion or pure exchange, respectively. The τ ratios, beam-size ratio, and their SEM were calculated from the experimentally measured τ and ω^2 values via bootstrap analysis (see Supplemental Experimental Procedures). This analysis showed that the τ ratio of WT ROP6 differs significantly from the 2.28 beam-size ratio predicted for FRAP by lateral diffusion (*$p \leq 0.02$; bootstrap analysis). The τ ratio of the $rop6^{CA21+156mSS}$ mutant differed significantly from both 2.28 ($p \leq 10^{-10}$; bootstrap analysis) and from 1, the value expected for FRAP by exchange (**$p \leq 10^{-3}$; bootstrap analysis).

The effect of transient *S*-acylation on vesicle uptake from the plasma membrane was evaluated by the change in intracellular FM4-64 fluorescence intensity in RHs at 3 min intervals (Figure 4C). In nontransgenic WT and *WT-ROP6* transgenic RHs, accumulation of FM4-64 reached saturation within 9 min, whereas in $rop6^{CA}$ RH, the endocytosis of FM4-64 was completely blocked. FM4-64 endocytosis in the C21S and C156S single and double mutants was attenuated in direct relation to their *S*-acylation level and effect on RH growth. In $rop6^{CA21mS}$ RH, fluorescence became visible after 20 min, with intensity that was approximately 20% of WT RH. In $rop6^{CA156mS}$ RH, fluorescence became visible after 12 min; after 20 min, the fluorescence intensity was 50% compared to WT. Similar to WT, in $rop6^{CA21+156mSS}$ RH, FM4-64 fluorescence became visible after 6 min but with a lower (~30%) intensity. After 9 min, the intensity was 50% compared to WT, reaching WT levels at 20 min (Figure 4C). The differences in ROS distribution were quantified by calculating the percentage of RH area covered by DCF-labeled ROS fluorescence with projection stack images (Figure 4D). Significant differences were detected between $rop6^{CA}$, $rop6^{CA156mS}$, $rop6^{CA21+156mSS}$, and WT nontransgenic plants ($p \leq 0.01$; ANOVA).

Epidermis pavement cell structure was also significantly different between the different lines ($p \leq 0.01$; ANOVA) (Figure 3C; Figure 4E). Importantly, expression of $rop6^{CA}$ from the *pROP6* or *35S* promoters induced similar depolarization of leaf epidermis pavement cells (Figure S2A). A scale termed

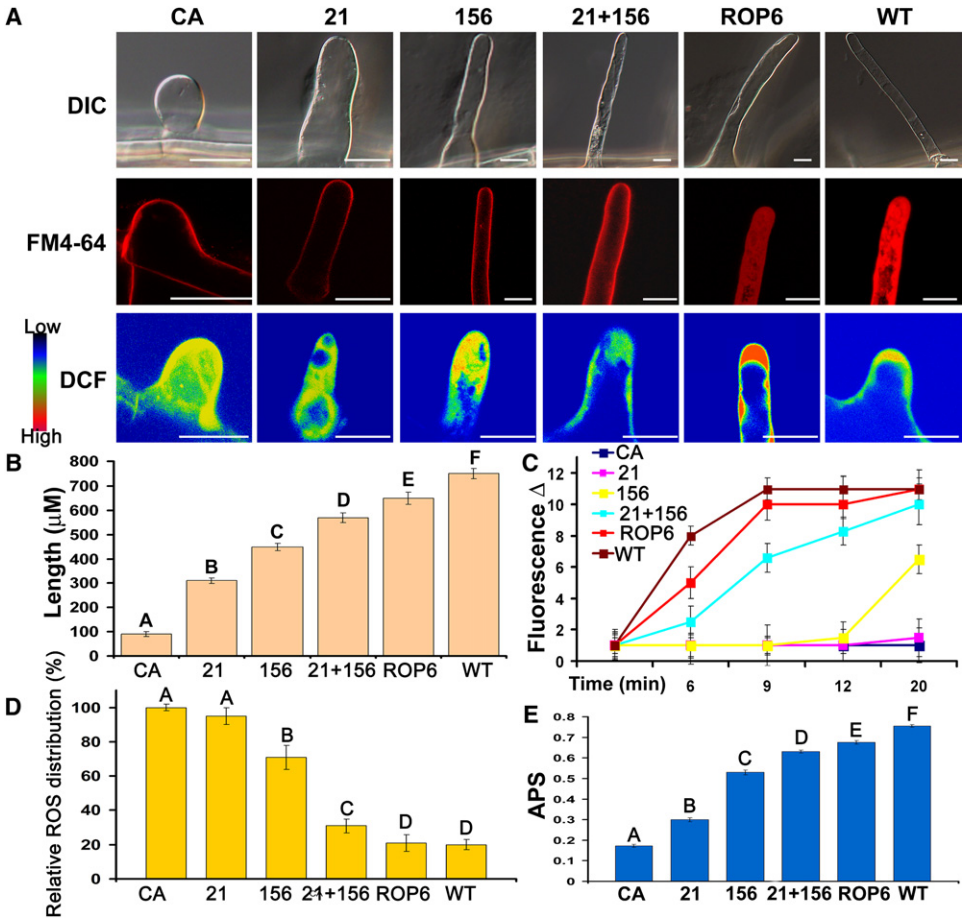

Figure 4. *S*-Acylation of C21 and C156 Is Required for ROP6 Signaling in Cell Polarity

(A–D) Effect of WT and mutant ROP6 on root hairs (RHs) phenotype.

(A) Differential interference contrast, FM4-64 (red) uptake, and DCF-labeled reactive oxygen species (ROS) distribution in RHs. Bars correspond to 100 μm in the DIC images and 40 μm in the FM4-64 and DCF-ROS images.

(B) RH length.

(C) Quantitative analysis of FM4-64 uptake.

(D) Percentage of RH area covered by DCF-labeled ROS fluorescence.

(E) Average polarity score (APS) values of leaf epidermis pavement cells. See also Figure S4 for skeleton endpoint and circularity data and explanation of APS calculation. Error bars in (B)–(E) correspond to SE. In (B), (D), and (E), letters above the bars denote significant differences ($p \leq 0.01$; ANOVA) between lines.

average polarity score (APS), which combined the ImageJ-based generated values of skeleton endpoints and circularity [25], was used for determining pavement cell structure (Figure S5). The APS scale ranges from 0 to 1, where 0 is a circular apolar cell and 1 is a polar cell with many long lobes (Figure S4A). The APS values of plant pavement cells were 0.75 and 0.68 in nontransgenic *WT* and *WT-ROP6* transgenic plants, respectively. In contrast, the APS value of *rop6*^{CA} pavement cells was 0.17 (Figure 4E). As for RH, reduction of the *S*-acylation levels in C21S and C156S single and double mutants corresponded with the change in APS values (0.29, 0.52, and 0.63 for *rop6*^{CA21mS}, *rop6*^{CA156mS}, and *rop6*$^{CA21+156mSS}$, respectively). These results demonstrate a positive correlation between *S*-acylation, localization in lipid rafts, and effects on cell polarity. In all cases, reduction in the *S*-acylation levels reduced the effect on cell polarity caused by the activated rop6^{CA} mutant. The results in Figure 4 show that *S*-acylation is required for ROP6 signaling during regulation of cell polarity. The differences in cell structure, FM4-64 endocytic uptake, and ROS distribution between *rop6*$^{CA21+156mSS}$ and both WT and ROP6 plants indicate that the CA rop6^{CA} mutant retains some acylation-independent activity.

The current results show that activation-coupled *S*-acylation of G domain C21 and C156 regulates signaling by *Arabidopsis* ROP6 and possibly other ROP and Rho GTPases. The following major conclusions can be drawn. Inspection of the protein structure (Figure 1) indicates that a conformational change is required for C156 *S*-acylation, suggesting that enzymatic activity, e.g., protein acyl transferase and/or other molecular factors, is needed to overcome the attendant energetic cost. Using Rac1-arfaptin crystal structures in both GDP and GTP states as models (PDB codes 1I4D, 1I4T) shows that effectors should not be hindered sterically in their access to switch regions. Surface access calculations show very little difference between the GDP and GTP states for both cysteines. Thus, further study will be required to examine whether and how *S*-acylation is nucleotide-state dependent. FRAP

beam-size analysis (Figure 3F) indicates that *S*-acylation contributes to the stabilization of ROP6 membrane interactions (loss of *S*-acylation increases the exchange rate), and Figure 3D demonstrates that it can also regulate ROP6 recruitment to lipid rafts. Finally, the Rho activation assay (Figure 3B) and the functional analyses (Figure 4) show that nonacylated ROP6 mutants retain basal activity, implying that they still interact with downstream effectors. Notably, *S*-acylation greatly enhanced activated ROP signaling, possibly by enhancing ROP partitioning into lipid rafts and stabilizing ROP-membrane interactions. Combined molecular dynamics simulations and fluorescence resonance energy transfer studies suggest that effector binding to GTP-bound Ras isoforms can occur concomitantly with plasma membrane interactions by G domain residues [26]. The evolutionary conservation of C21 and C156 suggests that transient *S*-acylation may not be restricted to plant Rhos.

Experimental Procedures

A detailed description of experimental procedures can be found in the Supplemental Experimental Procedures. Molecular cloning, transformation, and protein expression procedures followed standard protocols. All plasmids, oligonucleotide primers, and transgenic plant lines are listed in Tables S1–S3. Transformations of *Arabidopsis* were carried out via the floral dip method [27]. Protein expression in *E. coli* was previously described [11, 19]. Preparation of plant protein extracts, separation of membranes on sucrose density gradients, and fractionation of membranes with detergent were carried out as previously described [11]. Protein *S*-acylation was as described earlier [11, 17]. In GTPase activation assays, GST-ICR1 [19] was used to pull down GTP-bound ROPs. GTPase activity assays were performed with Enzcheck Phosphate Assay Kit (E-6646, Molecular Probes). Bound nucleotides were identified by HPLC, as previously described [15]. Imaging employed a Leica TCS-SL CLSM. Immunostainings [28] and labeling with FM4-64 [22] were as previously described. ROS labeling with DCF (Molecular Probes) FRAP beam-size analyses was conducted as described [13, 29, 30]. Leaf epidermis pavement cell skeleton endpoint and circularity were calculated with ImageJ as described [25], defining APS = (normalized circularity + normalized skeleton)/2; normalized circularity = 1 − circularity; and normalized skeleton = (skeleton score − 2)/14.

Supplemental Information

Supplemental Information includes Supplemental Experimental Procedures, four figures, and three tables and can be found with this article online at doi:10.1016/j.cub.2010.03.057.

Acknowledgments

We thank D. Szymanski and L. Hadany for advice and the Manna Center at the Department of Molecular Biology and Ecology of Plants at Tel Aviv University for equipment and growth facilities support. This work was supported by US-Israel Binational Agricultural Research and Development Fund (BARD-IS-4032-07), Israel Science Foundation (ISF-312/07), and the Deutschland-Israel Program (DIP-H.3.1) grants to S.Y. N.S. is supported by an Eshkol fellowship for PhD students from The Israel Ministry of Science and Technology and by a European Molecular Biology Organization short-term fellowship. Y.I.H. is an incumbent of the Zalman Weinberg Chair in Cell Biology.

Received: December 29, 2009
Revised: March 11, 2010
Accepted: March 13, 2010
Published online: May 6, 2010

References

1. Jaffe, A.B., and Hall, A. (2005). Rho GTPases: Biochemistry and biology. Annu. Rev. Cell Dev. Biol. *21*, 247–269.
2. Ridley, A.J. (2006). Rho GTPases and actin dynamics in membrane protrusions and vesicle trafficking. Trends Cell Biol. *16*, 522–529.
3. Nibau, C., Wu, H.M., and Cheung, A.Y. (2006). RAC/ROP GTPases: 'Hubs' for signal integration and diversification in plants. Trends Plant Sci. *11*, 309–315.
4. Yalovsky, S., Bloch, D., Sorek, N., and Kost, B. (2008). Regulation of membrane trafficking, cytoskeleton dynamics, and cell polarity by ROP/RAC GTPases. Plant Physiol. *147*, 1527–1543.
5. Yang, Z., and Fu, Y. (2007). ROP/RAC GTPase signaling. Curr. Opin. Plant Biol. *10*, 490–494.
6. Hancock, J.F., Paterson, H., and Marshall, C.J. (1990). A polybasic domain or palmitoylation is required in addition to the CAAX motif to localize p21ras to the plasma membrane. Cell *63*, 133–139.
7. Michaelson, D., Silletti, J., Murphy, G., D'Eustachio, P., Rush, M., and Philips, M.R. (2001). Differential localization of Rho GTPases in live cells: Regulation by hypervariable regions and RhoGDI binding. J. Cell Biol. *152*, 111–126.
8. Laude, A.J., and Prior, I.A. (2008). Palmitoylation and localisation of RAS isoforms are modulated by the hypervariable linker domain. J. Cell Sci. *121*, 421–427.
9. Lavy, M., Bracha-Drori, K., Sternberg, H., and Yalovsky, S. (2002). A cell-specific, prenylation-independent mechanism regulates targeting of type II RACs. Plant Cell *14*, 2431–2450.
10. Lavy, M., and Yalovsky, S. (2006). Association of Arabidopsis type-II ROPs with the plasma membrane requires a conserved C-terminal sequence motif and a proximal polybasic domain. Plant J. *46*, 934–947.
11. Sorek, N., Poraty, L., Sternberg, H., Bar, E., Lewinsohn, E., and Yalovsky, S. (2007). Activation status-coupled transient S acylation determines membrane partitioning of a plant Rho-related GTPase. Mol. Cell. Biol. *27*, 2144–2154.
12. Linder, M.E., and Deschenes, R.J. (2007). Palmitoylation: Policing protein stability and traffic. Nat. Rev. Mol. Cell Biol. *8*, 74–84.
13. Henis, Y.I., Rotblat, B., and Kloog, Y. (2006). FRAP beam-size analysis to measure palmitoylation-dependent membrane association dynamics and microdomain partitioning of Ras proteins. Methods *40*, 183–190.
14. Berken, A., and Wittinghofer, A. (2008). Structure and function of Rho-type molecular switches in plants. Plant Physiol. Biochem. *46*, 380–393.
15. Tucker, J., Sczakiel, G., Feuerstein, J., John, J., Goody, R.S., and Wittinghofer, A. (1986). Expression of p21 proteins in Escherichia coli and stereochemistry of the nucleotide-binding site. EMBO J. *5*, 1351–1358.
16. Spangler, C., Spangler, C.M., Spoerner, M., and Schäferling, M. (2009). Kinetic determination of the GTPase activity of Ras proteins by means of a luminescent terbium complex. Anal. Bioanal. Chem. *394*, 989–996.
17. Sorek, N., and Yalovsky, S. (2010). Analysis of protein *S*-acylation by gas chromatography-coupled mass spectrometry using purified proteins. Nat. Protoc. *5*, 834–840.
18. Grebe, M., Xu, J., Möbius, W., Ueda, T., Nakano, A., Geuze, H.J., Rook, M.B., and Scheres, B. (2003). Arabidopsis sterol endocytosis involves actin-mediated trafficking via ARA6-positive early endosomes. Curr. Biol. *13*, 1378–1387.
19. Lavy, M., Bloch, D., Hazak, O., Gutman, I., Poraty, L., Sorek, N., Sternberg, H., and Yalovsky, S. (2007). A novel ROP/RAC effector links cell polarity, root-meristem maintenance, and vesicle trafficking. Curr. Biol. *17*, 947–952.
20. Rotblat, B., Prior, I.A., Muncke, C., Parton, R.G., Kloog, Y., Henis, Y.I., and Hancock, J.F. (2004). Three separable domains regulate GTP-dependent association of H-ras with the plasma membrane. Mol. Cell. Biol. *24*, 6799–6810.
21. Prior, I.A., Harding, A., Yan, J., Sluimer, J., Parton, R.G., and Hancock, J.F. (2001). GTP-dependent segregation of H-ras from lipid rafts is required for biological activity. Nat. Cell Biol. *3*, 368–375.
22. Bloch, D., Lavy, M., Efrat, Y., Efroni, I., Bracha-Drori, K., Abu-Abied, M., Sadot, E., and Yalovsky, S. (2005). Ectopic expression of an activated RAC in Arabidopsis disrupts membrane cycling. Mol. Biol. Cell *16*, 1913–1927.
23. Jones, M.A., Shen, J.-J., Fu, Y., Li, H., Yang, Z., and Grierson, C.S. (2002). The Arabidopsis Rop2 GTPase is a positive regulator of both root hair initiation and tip growth. Plant Cell *14*, 763–776.
24. Foreman, J., Demidchik, V., Bothwell, J.H., Mylona, P., Miedema, H., Torres, M.A., Linstead, P., Costa, S., Brownlee, C., Jones, J.D., et al. (2003). Reactive oxygen species produced by NADPH oxidase regulate plant cell growth. Nature *422*, 442–446.
25. Le, J., Mallery, E.L., Zhang, C., Brankle, S., and Szymanski, D.B. (2006). Arabidopsis BRICK1/HSPC300 is an essential WAVE-complex subunit that selectively stabilizes the Arp2/3 activator SCAR2. Curr. Biol. *16*, 895–901.

26. Abankwa, D., Gorfe, A.A., Inder, K., and Hancock, J.F. (2010). Ras membrane orientation and nanodomain localization generate isoform diversity. Proc. Natl. Acad. Sci. USA *107*, 1130–1135.
27. Clough, S.J., and Bent, A.F. (1998). Floral dip: A simplified method for Agrobacterium-mediated transformation of Arabidopsis thaliana. Plant J. *16*, 735–743.
28. Richter, S., Geldner, N., Schrader, J., Wolters, H., Stierhof, Y.D., Rios, G., Koncz, C., Robinson, D.G., and Jürgens, G. (2007). Functional diversification of closely related ARF-GEFs in protein secretion and recycling. Nature *448*, 488–492.
29. Illenberger, D., Walliser, C., Strobel, J., Gutman, O., Niv, H., Gaidzik, V., Kloog, Y., Gierschik, P., and Henis, Y.I. (2003). Rac2 regulation of phospholipase C-beta 2 activity and mode of membrane interactions in intact cells. J. Biol. Chem. *278*, 8645–8652.
30. Eisenberg, S., Giehl, K., Henis, Y.I., and Ehrlich, M. (2008). Differential interference of chlorpromazine with the membrane interactions of oncogenic K-Ras and its effects on cell growth. J. Biol. Chem. *283*, 27279–27288.